Journal of Bio- and Tribo-Corrosion (2020) 6:124
https://doi.org/10.1007/s40735-020-00421-3

Microstructural and Tribological Resistance of Flame-Sprayed CoMoCrSi/WC-CrC-Ni and CoMoCrSi/WC-12Co Composite Coatings Remelted by Microwave Energy

C. Durga Prasad[1] · Sharnappa Joladarashi[2] · M. R. Ramesh[2] · M. S. Srinath[3]

Received: 11 April 2020 / Revised: 20 August 2020 / Accepted: 4 September 2020 / Published online: 12 September 2020

Abstract
The hard facing composite coatings such as CoMoCrSi/30%WC-CrC-Ni and CoMoCrSi/30%WC-12Co are coated on grade-2 titanium substrate through Flame spray technique. Prior to deposition of coatings CoMoCrSi feedstock were processed using high energy ball milling to obtain intermetallic laves phases. The sprayed coatings are subjected to post-heat treatment through microwave energy to homogenize coating structure which reduces surface defects and to achieve metallurgical bonding. The as-sprayed and microwave treated coatings are examined for metallography analysis by using XRD, SEM–EDS and mechanical properties are estimated by using microhardness, universal tensile equipment. The high-temperature sliding wear tests are performed against alumina counterpart under dry conditions. The sliding wear test is conducted with normal loads of 10 N and 20 N at a sliding velocity of 1.5 m/s with a constant sliding distance of 3000 m. Microwave treated coatings obtained homogeneous structure and metallurgical bonding with improved hardness. Fused coatings revealed better wear resistance due to formation of oxides and fatigue spalling mechanism.

Keywords CoMoCrSi · Homogenize · Flame spray · Microwave energy · High-temperature wear

1 Introduction

The surfaces of titanium and most of its alloys have relatively poor wear resistance and also it is prone to oxidation and oxygen-induced embrittlement at temperatures above 600 °C [1]. All materials do wear to some extent and usual solution to minimize that is the proper configuration of mating surfaces or wise choice of lubricants [2]. In metals, wear usually occurs by plastic displacement and detachment of the surface particles. Wear rate is affected by many factors such as, the type of loading, type of motion and temperature. Loading may be of static, dynamic, impact and motion may be of sliding, rolling [3].

The cost of engineering material loss due to several surface degradations may reach 4% of gross internal product (GIP) is facing by most of the countries. For instance, in the United States alone it is seen that the wear and corrosion of spare parts cost around 22 billion Euros per year [4]. Besides this, an indirect cost involved in the production, scrap management, maintenance, adds up to the cost of material and thereby increases the cost of the material. To overcome these tribological problems, the demand for new alternatives has increased in recent times [5].

Nowadays, surface modification is mainly done by depositing the coating materials, usually hard and corrosion resistant materials on the surface of ductile materials that are prone to corrosion and wear attack. In these surface coating technologies, the properties of the deposited coatings are quite different from that of the substrate materials. This approach also enables the use of economical materials for the components which also results in better properties by modifying the surface of the substrate.[6–9].

Thermal spray coatings belong to the surface modification techniques, in which the coating material is applied

✉ C. Durga Prasad
durgaprasi71@gmail.com

1 Department of Mechanical Engineering, RV Institute of Technology and Management, Bengaluru, Karnataka 560076, India

2 Department of Mechanical Engineering, National Institute of Technology Karnataka, Surathkal 575025, India

3 Department of Industrial and Production Engineering, Malnad College of Engineering, Hassan, Karnataka, India

onto the surface so as to obtain thick wear resistant surfaces [10]. It improves the lifetime of materials and enhances the performance of the components, by adding functionality to the surfaces. One major advantage with thermal coatings is that variety of materials, ranging from soft plastics to hard refractory materials could be deal to produce hard films for multiple applications. The versatility of the process makes it suitable for use against wear, high-temperature environments, corrosion, repair and restoration of parts [11, 12]. However, the as-sprayed coating exhibits several interface defects which strongly effects on its surface properties leads to decrease in component efficiency. Spray process usually produces various sub surface defects which results in decrease in efficiency of the component. It is possible to eliminate defects from developed coating components through secondary heat treatment process.[13–16]. There are various existing methods under secondary heat treatment process are laser technique, electron beam method and furnace heat treatment [17]. These techniques are bit costlier, takes much longer time to complete the treatment and also it greatly effects on base metal properties. Implementing of new technology like microwave heating of materials which is having a provision of re-heating of sprayed coatings to impart desired properties. This method is very efficient which takes less duration to achieve heat and also it will not create any problems with base metal properties [18, 19].

There have been enough studies were done on the nickel and iron based materials and also many researchers have performed wear studies by employing various combination of cermets and ceramics. Nickel, tungsten based carbides are comparatively costlier and dealing with cermets/ceramics are very difficult due to its hard nature properties. However, usage of metallic materials under similar applications would be best solution to reduce cost as well as it is easy to perform secondary operations [20, 21]. Nowadays cobalt based metallic materials are extensively using in many applications such as batteries, marine, automobile and oil industries because of its superior high-temperature strength and chemical properties [22–24]. Cobalt based powder with comprising of molybdenum, chromium and silicon (CoMoCrSi) would provide higher hardness, elevated temperature wear resistance as well as chemical stability due to presence of intermetallic laves phases in it [22, 23].

The present studies explore the new technique of milling the CoMoCrSi (Tribaloy T400) matrix feedstock to obtain intermetallic phases. The carbide powders like WC-12Co and WC-CrC-Ni are reinforced into milled CoMoCrSi feedstock individually. The CoMoCrSi + (30%) WC-CrC-Ni and CoMoCrSi + (30%) WC-12Co feedstocks are sprayed on titanium substrate by using flame spray technique. Microwave energy technique is utilized to remelt the deposited coatings. The coatings before and after fusing are subjected to various characterization techniques to analyze their metallurgical and mechanical properties. The elevated temperature wear resistances of both coatings are tested under dry sliding conditions.

2 Materials and Methods

2.1 Preparation of Feedstock and Composite Coatings

The titanium grade -2 is used as the substrate. The substrate is cut to standard size of 12 mm × 12 mm × 5 mm. The base powder CoMoCrSi is milled for the period of 5 h by high energy ball milling (HEBM) process. The detailed procedure and mechanism of milling of CoMoCrSi are discussed in the article [22]. Prior to milling, CoMoCrSi particles are having a size of 53–150 µm. The particle size of cermet powders of 45 + 15 µm are reinforced into milled CoMoCrSi powder individually as per weight ratio of 70: 30. The composite feedstock 40.71Co-20.65Mo-6.65Cr-1.98Si/21.9WC-6CrC-2.1Ni (70%/30%) and 40.71Co-20.65Mo-6.65Cr-1.98Si/26.4WC-3.6Co (70%/30%) are made to deposit on titanium substrate using flame spray method. The CoMoCrSi/WC-CrC-Ni and CoMoCrSi/WC-12Co will be referred as coating 1 and coating 2 in the further sections.

The deposition of coatings is done by using SPRAY-TORCH-100 gun flame spray method. Prior to coat, the substrate sample is subjected to primary preparations like cleaning and creating rough surface by Al_2O_3 grit blasting method. This results in better bonding of the coating with the target element. The combustion gas (oxy-acetylene) is used to produces heat in the spray gun. The spray torch supplies heat and made to melt the composite feedstock. The molten particles are sprayed at a low acceleration which deposits over the titanium substrate. The deposited composite coating is allowed to cool under atmospheric conditions. The key parameters employed for flame spray system includes oxygen flow: 45 lpm, fuel-acetylene: 55 lpm, powder rate: 38 g/min, oxygen and acetylene pressure: 2.1 and 1.1 kg/cm^2 and spray distance: 10 cm. These spray parameters have selected based on literature review as well as industrial experts such as (Hoganas and MEC) [9, 12–17].

The as-sprayed coatings are remelted using domestic microwave unit (LG, India, Solar Dom Model No: ML-3483FRR). The optimum temperature required to fuse the as-sprayed coating is 900–950 °C using microwave energy. The similar work has been carried out by author and the procedure of test is reported clearly in articles [18, 22, 23].

2.2 Characterization of Composite Feedstock and Coatings

The microstructure of feedstock and morphologies (cross-section and surface) of coatings are investigated by SEM attached with EDS (JOEL-JSM-6380LA, Japan). The composite coatings before and after microwave treatment are subjected to surface roughness measurement and porosity analysis by stylus type roughness instrument (TR-200, range 0.05–15 μm) and image analyzer software (ARTRAY , AT 130, Japan) respectively. The porosity is measured at 20 various locations and the average value is stated. The phase analysis of composite feedstock and composite coatings before and after treatment are examined by X-ray diffraction technique (Rigaku Miniflex diffractometer). The microhardness and adhesion strength of composite coatings with and without post treatment are conducted by employing Vicker's microhardness and pull-off test (ASTM C 633–13) methods respectively. The microhardness is measured on an OMNITECH, S-AUTO unit using 300 g load and a loading time of 30 s, and average of 20 readings is reported. The adhesion strength of composite coatings is estimated by the ratio of maximum load to cross-sectional area with a constant strain rate of 0.5 mm/min using Universal testing machine (Shimadzu hydraulic tensile machine). Adhesive bond of FM 1000 epoxy resin is applied between coating and counterpart. The mean value of 4 replicates is stated.

2.3 Sliding Wear Test

The high-temperature sliding wear test as per ASTM G-99 standards is performed on the substrate, as-sprayed and post treated composite coatings against alumina counterpart material using a pin on disc tribometer Ducom instruments Pvt. Ltd., Bangalore, INDIA (TR-20LE-PHM 400-CHM 600). The parameters such as normal load and test temperatures are varied, whereas sliding speed is kept constant throughout the test. The sliding wear tests are done on samples ($12 \times 12 \times 5$ mm^3) using a sliding velocity of 1.5 m/s, rotational speed of 238 rpm, a sliding distance of 3000 m (time: 34 min.) under loads of 10 and 20 N at temperatures of 200 °C, 400 °C and 600 °C. The wear rate of tested samples is computed by the volume loss method [11, 22, 23]. Three different samples of coatings are repeated in order to find the mean values. The tested samples are investigated through XRD, SEM–EDS process in order to analyze the mechanism of wear.

3 Results and Discussions

3.1 Feedstock Morphology

Figure 1a represents the microstructure of CoMoCrSi feedstock before the milling process. These particles are produced by a gas atomized technique which is having clear spherical shape. The cermet powders WC-CrC-Ni and WC-12Co are produced by agglomeration and sintered method having a spherical structure as shown in Fig. 1b and c. The microstructure of milled feedstock after 5 h duration is depicted in Fig. 1d. When the CoMoCrSi feedstock is subjected to milling operation, the particles experienced series of morphology changes like flattening, cold welding, plastic deformation, and fracture. During milling, due to the high impact energy applied continuously on particles results in changing its microstructure as well as a reduction in particles size from 53 to 150 μm to 60.12 μm. Manufacturing of feedstock mechanism has been discussed by Prasad et al. (2018) [22].

3.2 Morphology of Coatings

3.2.1 Microstructure of CoMoCrSi/WC-CrC-Ni (Coating 1)

The cross-section morphologies of coating 1 before and after treatment are shown in Fig. 2a and b. The as-sprayed coating reveals the presence of cracks and pores throughout the thickness of the coating in Fig. 2a. There is no such cracks have found and obtained better adhesion between coating and substrate. The number of coating layers applied on substrate to build the uniform coating thickness. The thickness is measured on different spots of coatings which confirm that there is no significant variation in thickness value results in uniform coating structure. The coating having a roughness and thickness are 14.45 μm and 210 μm respectively. The porosity is $9.54 \pm 1.25\%$. The post treated coating exhibits significant changes in terms of microstructural features such as reduced cracks and voids results in a homogeneous structure in Fig. 2b. The heat treated coating having a roughness and thickness are 6.28 μm and 235 μm respectively. The porosity of heat treated coating is $3.15 \pm 0.9\%$. The transition of substrate element into coating region at interface region results in metallurgical bounding.

The surface morphology of coating 1 before and after treatment and its EDS analysis are presented in Fig. 3a and b. The unmelted and semi-melted particles can be observed in the surface of as-sprayed coating Fig. 3a. The spray process employed in this work produces less velocity due to these coating particles remains partial melted on the surface of the substrate. The EDS analysis of the as-sprayed coating describes the presence of cobalt-rich element along with reinforced carbides and also confirms the presence of oxides on the surface of coating in Fig. 3a. The fused coating surface morphology and its EDS analysis are depicted in Fig. 3b. The surface shows proper remelting of coating with eliminating unmelted and partial melted particles in Fig. 3b. The remelted coating surface has oxide stringers because of air induced into coating during spraying. The substrate element titanium is identified by EDS analysis of fused coating

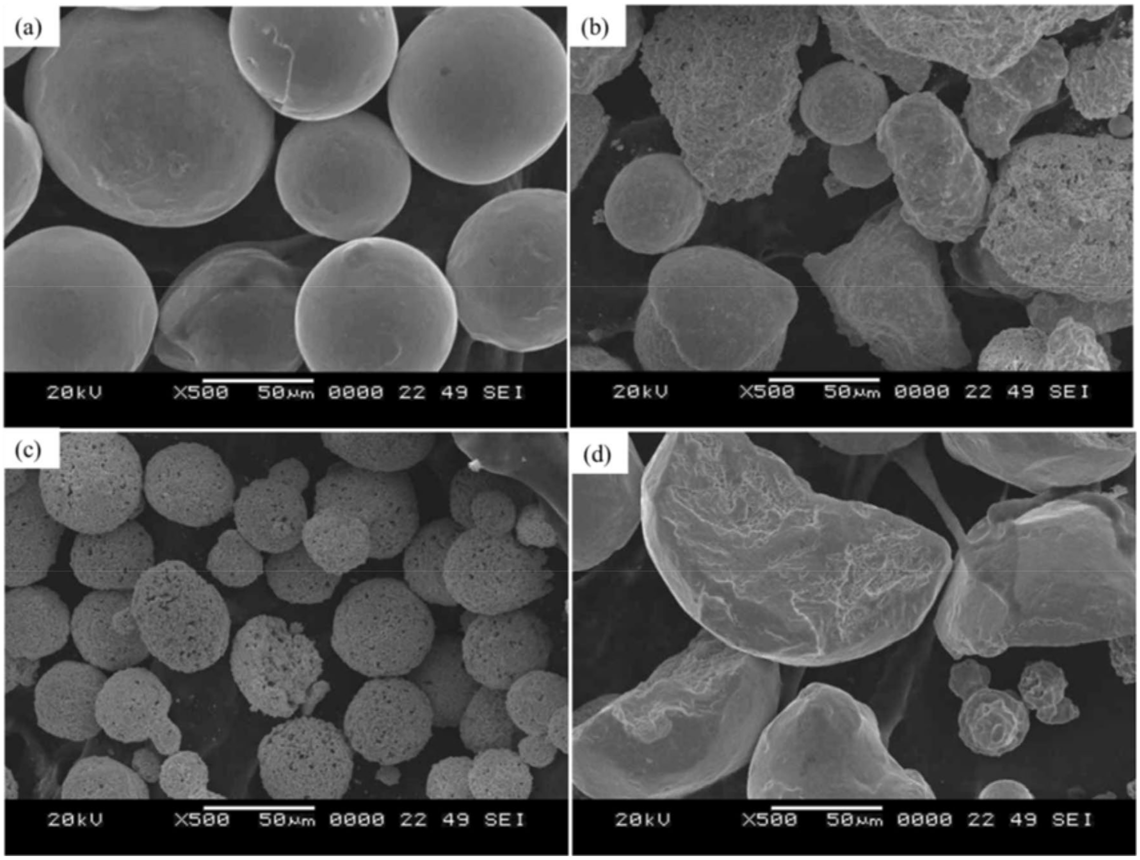

Fig. 1 Microstructures of feedstock **a** CoMoCrSi before milling **b** WC-CrC-Ni. **c** WC-12Co **d** CoMoCrSi after milling

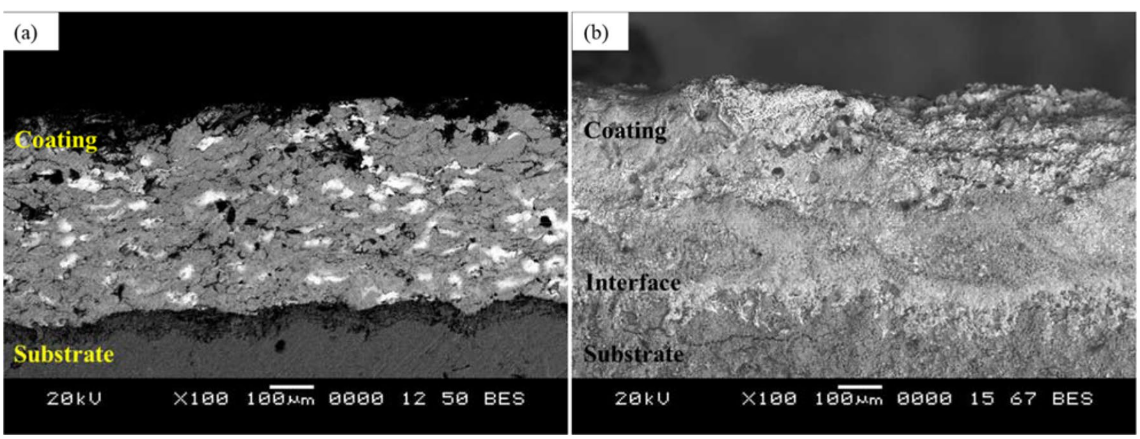

Fig. 2 SEM cross-section micrograph of coating 1 **a** as-sprayed **b** fused

due to diffusion. This is the effect of post treatment process. Also, the percentage of oxide element is increased and observed no significant changes in the percentage of other major coating elements.

3.2.2 Microstructure of CoMoCrSi/WC-12Co (Coating 2)

The cross-section morphologies of coating 2 before and after post treatment are shown in Fig. 4a and b. The as-sprayed coating cross-section has many defects like voids in between splats, semi-melted particles, and large cracks

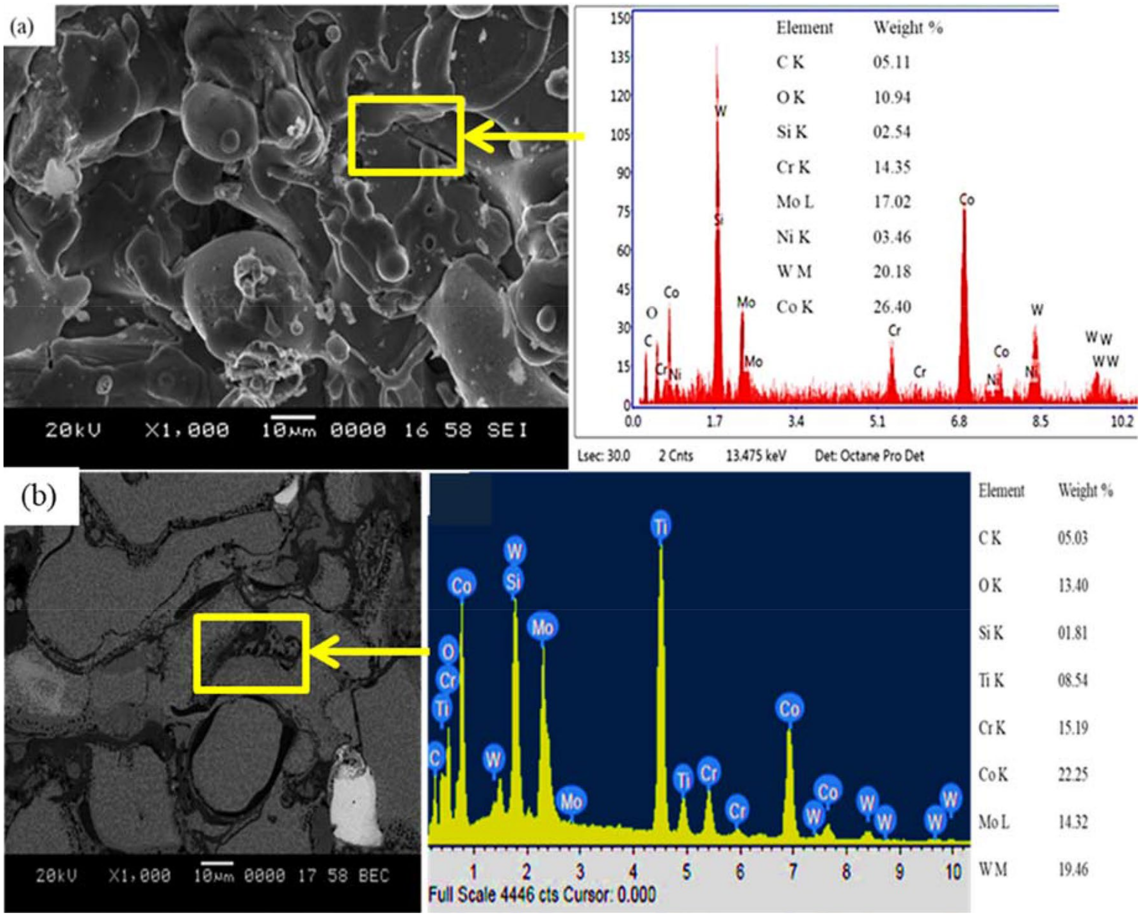

Fig. 3 Surface morphology of coating 1 **a** as-sprayed **b** fused

have observed and also a variation of coating structure can be seen in Fig. 4a. As-sprayed coating reveals the thickness and roughness are 176 µm and 11.32 µm respectively. Before treatment coating produced higher porosity is 11.05 ± 1.10%. The white patches in the coating (Fig. 4a) represents the chromium element is surrounded by other major coating constituent elements. However, the cross-section of fused coating shows the homogeneous structure. After remelting, the coating fills the discontinuities and voids caused during spraying results in a reduction of porosity see in Fig. 4b.

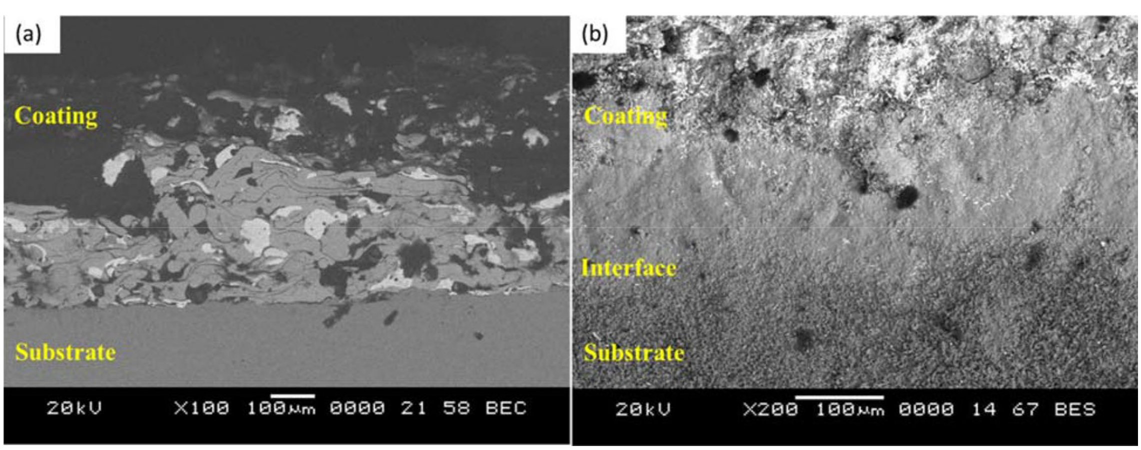

Fig. 4 SEM cross-section micrograph of coating 2 **a** as-sprayed **b** fused

The measured roughness and thickness of the treated coating is 5.50 µm and 192 µm. The assessed porosity of the fused coating is 4.42 ± 0.75%. The fused coating refines the microstructure of as-sprayed coating results in a reduction of surface roughness, porosity. The atomic diffusion near the interface zone (Fig. 4b) is observed due to remelting effect results in a slight increase in coating thickness made by the microwave heating process.

The surface micrographs of coating 2 before and after post treatment with its EDS reports are shown in Fig. 5a and b. The surface structure of the as-sprayed coating exhibits unmelted particles with large voids in Fig. 5a. The cobalt and tungsten are the dominant elements present in the as-sprayed coating revealed by the EDS report in Fig. 5a. The presence of oxide and carbides acts as a strengthener in the coating. The effect of microwave volumetric heating leads to complete remelting of fused coating and its surface reveals least defects with no existence of unmelted/semi-melted particles Fig. 5b. The EDS of fused coating presents an increase in the percentage of oxide and carbon elements due to oxidation and graphite sheet effect respectively. EDS results also reported the substrate element with prime constituents of coating shown in Fig. 5b.

3.3 Phase Analysis

The XRD patterns of coating 1 before and after post treatment depicts in Fig. 6a and b. The as-sprayed coating spectrum has a sharp crystalline structure with lower intensity. The pattern exhibits intermetallic phases such as Co_3Mo_2Si, Co_7Mo_6, and Co_2Mo_3. At 52°, 63° and 72° showed W_2C peaks, whereas Cr_3C_2 peaks are observed at 36°, 45°, and 50°. XRD spectrum of microwave fused coating 1 is shown in Fig. 6b. After post-heat treatment significant changes in pattern and also a slight broadening of peaks has been noticed see in Fig. 6b. The fused coating retains the similar phases as observed at as-sprayed and two new phases TiC and TiO_2 have been identified by a diffusion process. The new phases such as Co_6W_6C, Co_3W_9C, and Co_3W_3C are recorded which is represented by the symbol "♥" in Fig. 6b.

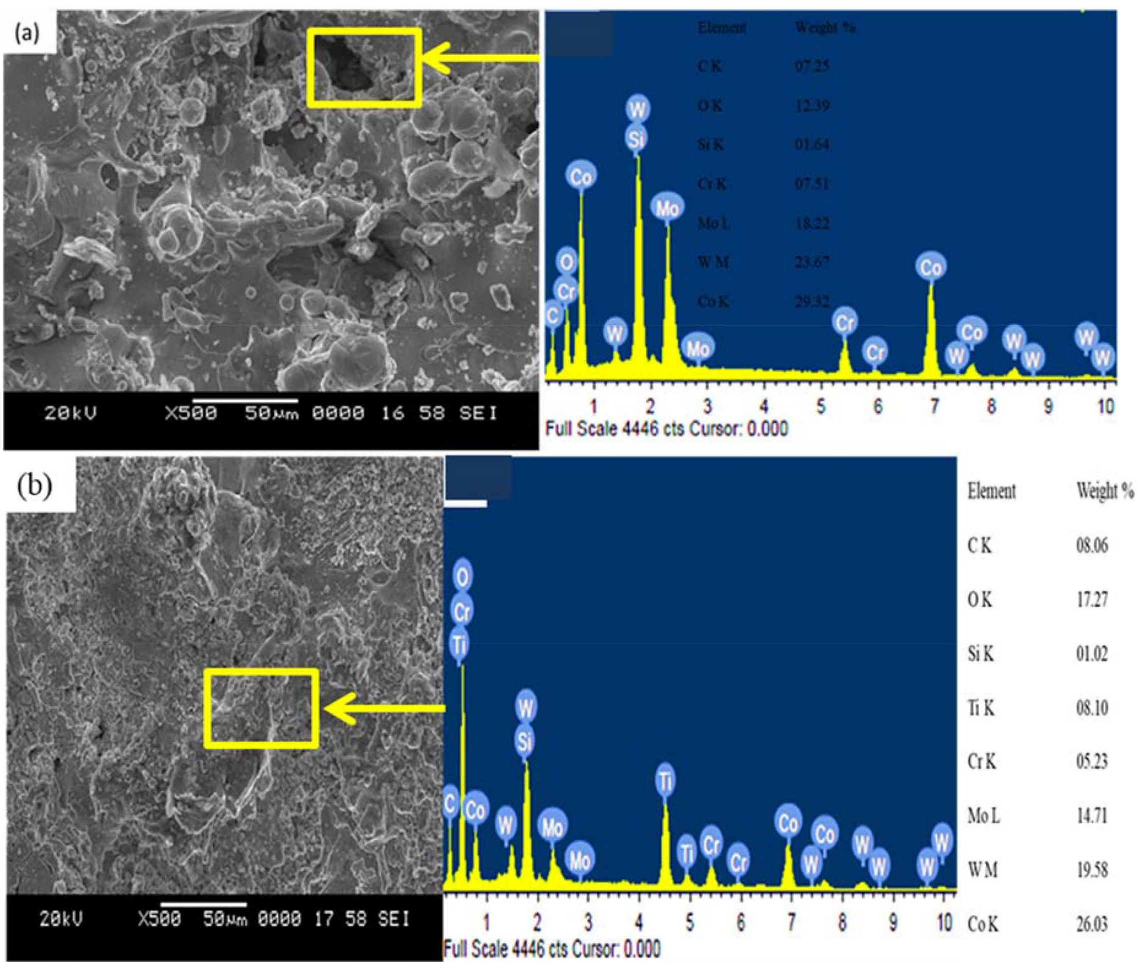

Fig. 5 Surface morphology of coating 2 **a** as-sprayed **b** fused

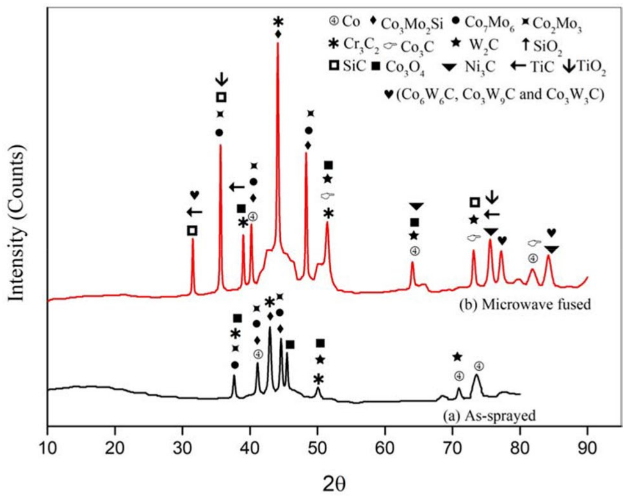

Fig. 6 XRD pattern of coating 1 **a** As-sprayed **b** Microwave fused

These phases strongly influence the coating properties reported by several researchers [24, 25]. The low velocity of the flame spray and fusing process subjected to oxidation results in the formation of oxide phases has been detected in its XRD pattern. The inducing of carbon to the as-sprayed coatings leads to increase in carbides percentage.

The XRD pattern of coating 2 before and after post treatment is presented in Fig. 7a and b. The XRD spectrum of the as-sprayed coating has broadening peaks due to amorphous structure of cobalt solid solution. This confirms the presence of intermetallic laves phase as discussed for Fig. 6 XRD profile. The W_2C phase is identified at 38°, 54° and 62° the Cr_3C_2 peak is observed at 40°, 48° and 54°. The fused coating has changed in its pattern structure due to volumetric heating effect by microwave process. The fused coating retains all the phases identified at as-sprayed coating with higher intensities. The other carbides such as Co_3C and SiC are existed and also oxide phases Co_3O_4 and SiO_2 are found. The addition of carbides produces new phases which are denoted by the symbol "♥" in Fig. 7b. The existence of these phases strengthens the coating hardness, high-temperature wear resistance properties. Substrate element (titanium) is transferred into interface region during remelting results in TiC and TiO_2 phases are formed.

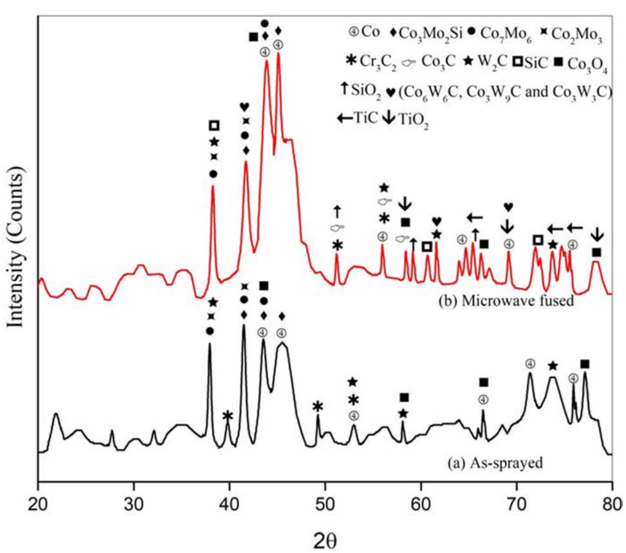

Fig. 7 XRD pattern of coating 2 **a** As-sprayed **b** Microwave fused

3.4 Evaluation of Microhardness and Adhesion Strength

Figure 8 presents the microhardness plots of coating 1 and coating 2. The measured average microhardness of coating 1 as-sprayed is 915 ± 33 HV and fused is 1156 ± 24 HV. Substrate exhibits a lower hardness of 183 ± 15 HV. The percentage of increase in hardness of coating 1 for fused sample over the as-sprayed sample is 26.33%. On other hand microhardness of coating 2 as-sprayed is 1050 ± 18 HV and fused is 1387 ± 30 HV. The percentage of increase of coating 2 for fused sample hardness over the as-sprayed sample is 32.09%.

In case of both as-sprayed coating 1 and 2, near interface zone hardness is slightly increased due to treatment with abrasive particles prior to coating. The hardness is varying with corresponding to thickness and hardness is started decreasing near-surface region of coatings. This is because of compressive stresses acting in between splats at the interface zone enhances hardness at interface zone whereas hardness is decreasing in between coating layers due to tensile stresses [3, 6]. Similarly in the case of both fused coating 1 and 2 experienced fluctuations in hardness values due to

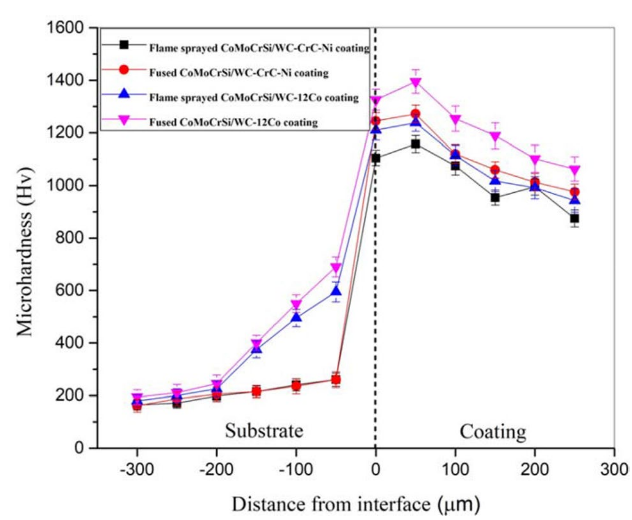

Fig. 8 Cross-section microhardness report of coatings

compressive and tensile stresses phenomenon [3, 6]. However, the hardness of fused coatings at the interface is high due to metallurgical bonding. Since the coating comprises of cobalt-rich solid solution intermetallics embedded into cermet reinforcements of WC-12Co coating 2 exhibits higher hardness than coating 1.

The adhesion strength of coating 1 and coating 2 before and after the post treatment are assessed. Figures 9 and 10 depict the fractured surface of coating 1 and coating 2 respectively. The adhesion strength of coating 1 as-sprayed is 32.18 ± 3.11 MPa and fused is 49.74 ± 1.56 MPa. It is clearly evidence that after microwave heating of coating 1, adhesion strength is significantly increased by 54.56% due to good metallurgical bonding. Similarly adhesion strength of coating 2 as-sprayed is 35.49 ± 2.83 MPa and fused is 54.04 ± 1.04 MPa. Adhesion strength of microwave treated coating 2 is increased by 52.26% due to transition of substrate element to coating and fine micrstructure. The fractured surface of both coatings (Figs. 9a, b and 10a, b) exhibits failure caused due to the failure of adhesive between substrate and coating.

3.5 Wear Behavior

3.5.1 Wear Comparison Studies of Coating 1 and Coating 2

Figure 11a and b represents the wear results in terms of volume loss of both coatings 1 and 2 at 10 N and 20 N normal load conditions. The substrate produces higher loss of volume corresponding to study temperature under both test loads. This confirms that as an increase in load and temperature, titanium substrate subjected to severe material loss under 20 N normal load at 600 °C. Both as-sprayed coatings 1 and 2 exhibit an increasing trend in loss of volume due to rough surface and presence of unmelted or semi-melted particles leads to easy deformation during sliding action under test loads. However, the presence of intermetallic phases and formation of metallurgical bonding in both fused coatings 1 and 2 results in less volume loss for both test loads compared to as-sprayed coatings 1 and 2 [26].

The wear rate of coatings and substrate are calculated using volume loss and sliding distance. The estimated wear rate of coatings and substrate are shown in Fig. 12a and b.

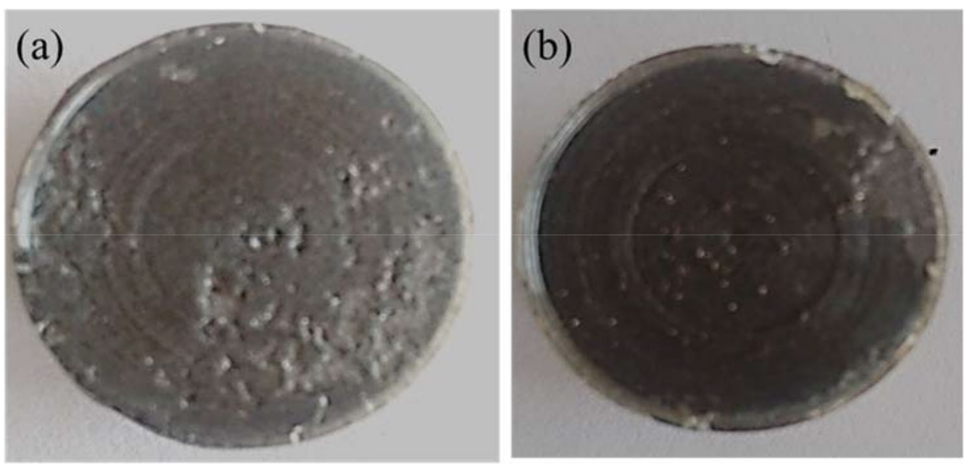

Fig. 9 Adhesion samples morphology of coating 1 **a** as-sprayed **b** fused

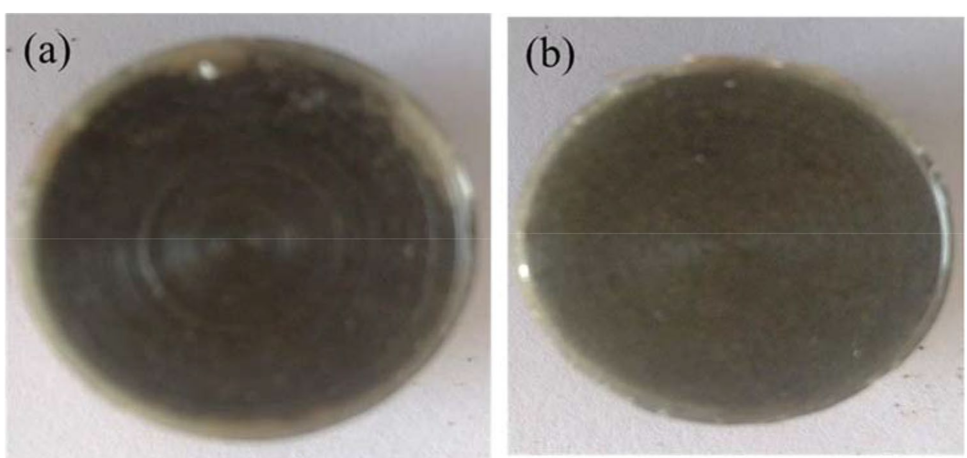

Fig. 10 Adhesion samples morphology of coating 2 **a** as-sprayed **b** fused

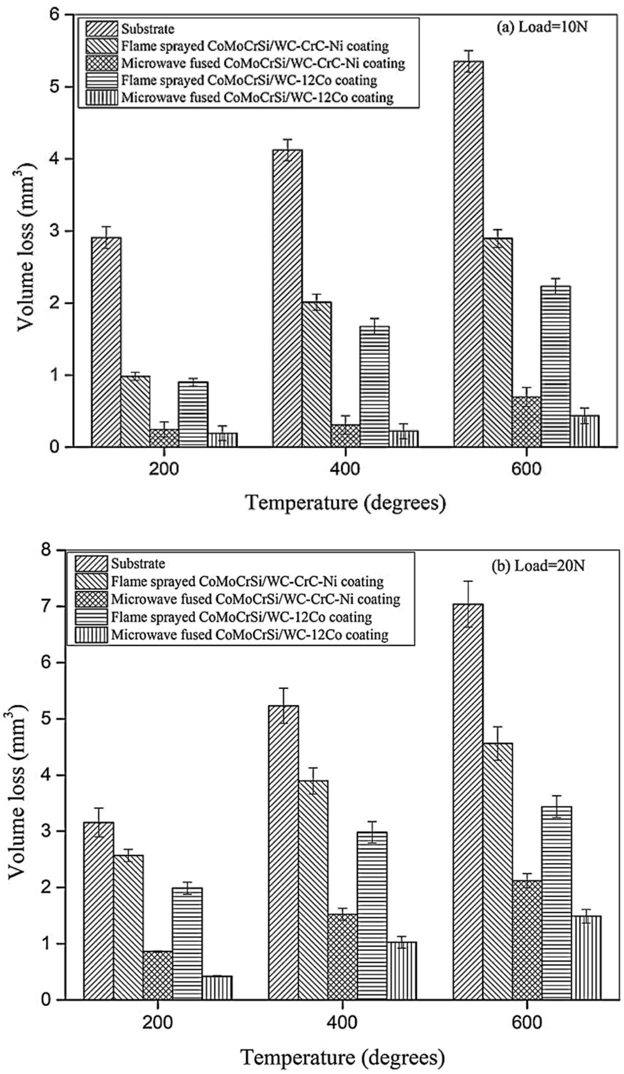

Fig. 11 Wear volume loss with respect to temperature **a** 10 N, **b** 20 N

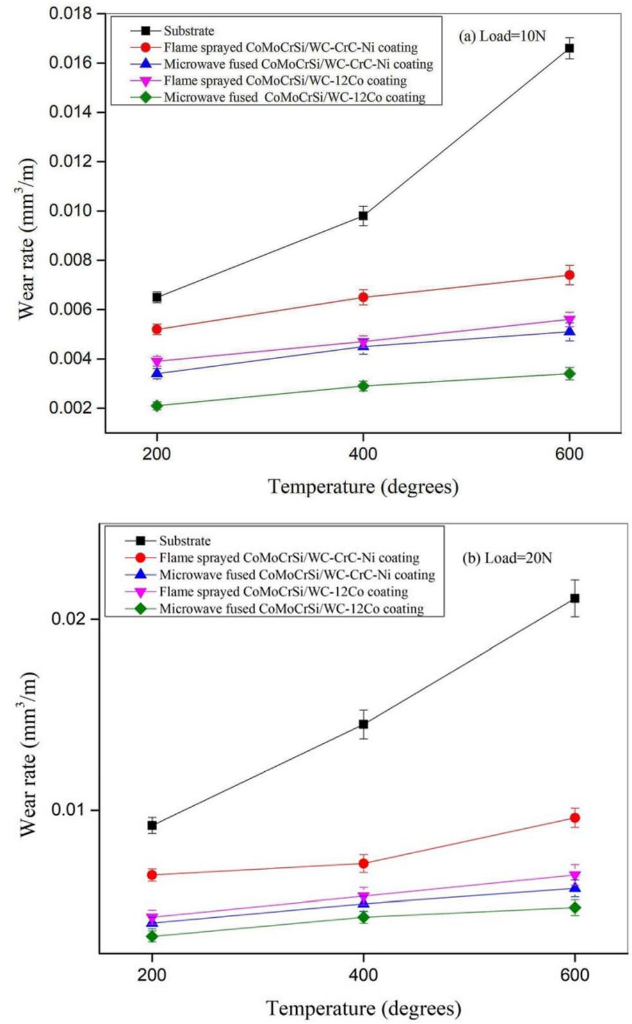

Fig. 12 Wear rate with respect to temperature **a** 10 N, **b** 20 N

As observed in Fig. 18a and b the substrate hardness is dominating by test temperature and load results in higher wear rate. The as-sprayed coating 1 produced wear rate of 2–2.5 times higher than fused coating 1 under both test loads. This is due to the heterogeneous structure of coating which has more pores, cracks as well as lower microhardness. In the case of as-sprayed coating 2 presents approximately 1–1.5 times higher wear rate than fused coating 2 for applied loads.

Since the microhardness of as-sprayed coating 2 is higher than as-sprayed coating 1 results in less rupture of material. Coating 2 exhibits better wear resistance than coating 1 based on the results of wear rate. The fused coating 2 produces 3.5–4 times lower wear rate than fused coating 1. The post treatment of coating has a lower wear rate due to enhanced hardness by diffusion mechanism and obtained phases such as TiC, TiO_2, Co_6W_6C, Co_3W_9C, and Co_3W_3C Cr_3C_2 are formed see in Figs. 6b and 7b. Also, the presences of intermetallic amorphous phases like (bulk metallic glass structure) and oxide phases formed during the sliding test play a role in reducing the wear rate of treated coatings.

3.5.2 Coefficient of Friction (COF)

Figure 13a and b shows the coefficient of friction (COF) of as-sprayed and fused coating 1. The COF of the as-sprayed coating 1 is significantly varying corresponding to the sliding distance. This is maybe contacted between coating sample and counter disc during sliding operation and presence uneven surface of the coating. The average COF of the as-sprayed coating under both test loads exhibits 0.65. The COF of as-sprayed coating 1 at 400 °C and 600 °C temperatures showed less value than 200 °C temperature. This is due to the formation of oxides near the coating surface at elevated temperatures leads to a decrease in friction [27–30]. The fused coating 1 tends to show lower COF of 0.51 which is

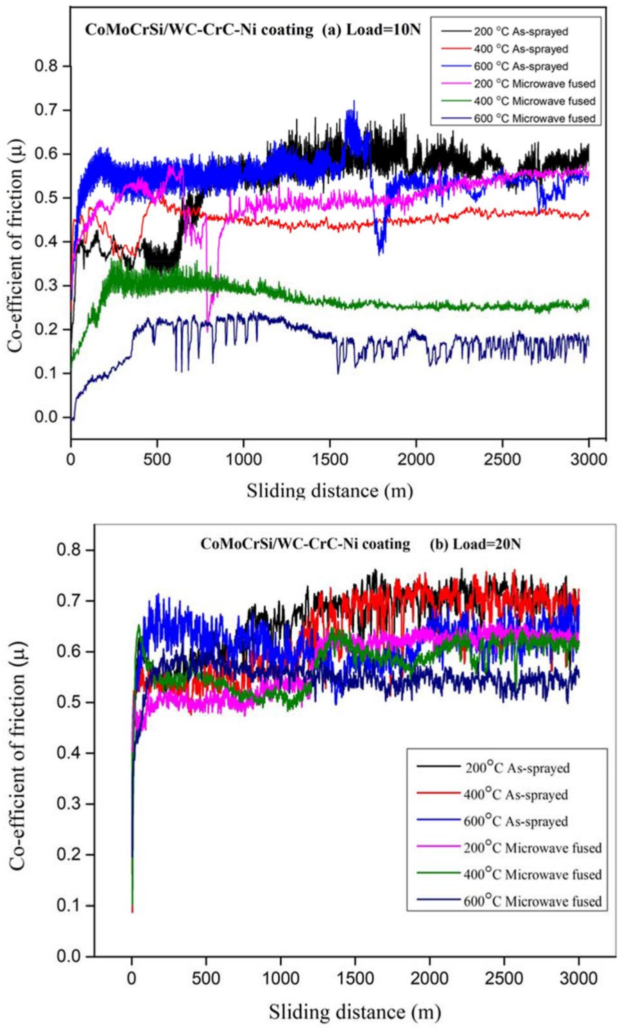

Fig. 13 COF of as-sprayed and fused coating 1 **a** 10 N, **b** 20 N

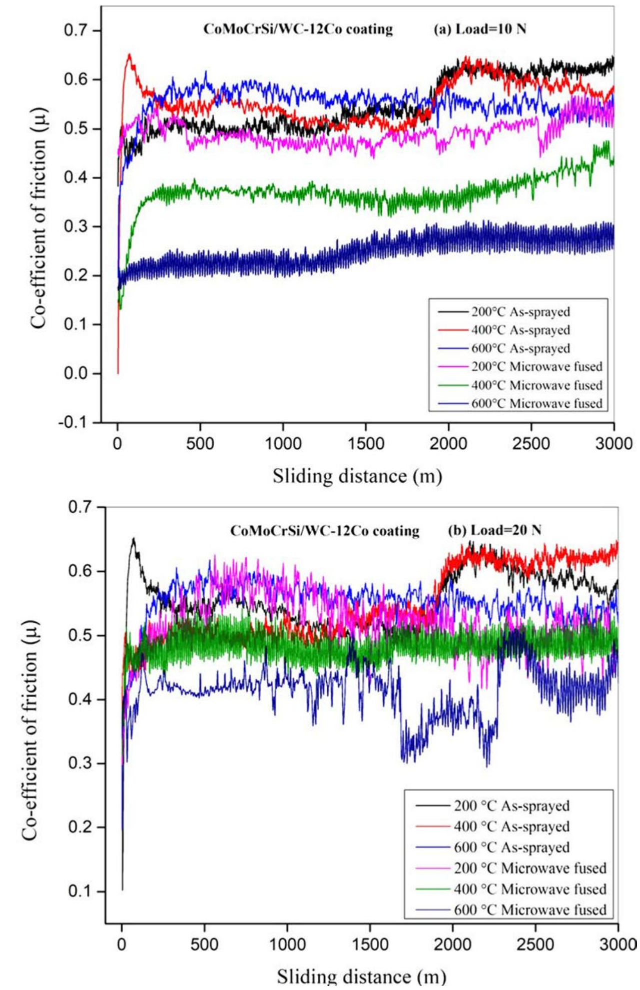

Fig. 14 COF of as-sprayed and fused coating 2 **a** 10 N, **b** 20 N

better than as-sprayed coating 1. Also, the fused coating 1 displays steady friction at all test temperatures. The homogeneous structure and presence of intermetallics result in the smooth flow of friction. But under 20 N normal load (Fig. 13b) both as-sprayed and fused coating 1 indicates more fluctuations of COF due to more applied force. Though at elevated temperatures fused coating 1 subjected to severe oxidation results in a reduction in COF. The oxides films are formed at elevated temperatures cover the fused coating 1 surface from breaking of material [31].

Figure 14 shows the COF of as-sprayed and fused coating 2. The COF of the as-sprayed coating is unstable throughout the sliding action. The mean COF value of as-sprayed coating 2 is 0.58, whereas fused coating 2 exhibits a stable friction curve having an average COF is 0.42, this is lower than as-sprayed coating 2 COF. The friction of as-sprayed and fused coating 2 at 200 °C temperature showed slightly higher value, but once the rise in temperature observed a decreasing trend in COF for fused coating 2. This is mainly due to the role of oxide layers formed near the coating surface at 400 °C and 600 °C temperatures. Also noticed that compared to 10 N normal load, as-sprayed and fused coating 2 are varying significantly in its COF under 20 N normal load in Fig. 14b. The increase in the contact force between sample and counter disc leads unstable in COF profiles.

3.5.3 XRD Analysis of Worn surface

The XRD pattens of fused coating 1 and coating 2 are shown in Figs. 15 and 16 respectively. Since the test is carried out at elevated temperatures obviously, Co alloy is subjected to oxidation at elevated temperatures and easily forms oxides at coating surfaces [32–34].

In Figs. 15 and 16, observed Co_7Mo_6 and Co_3O_4phases to be formed at 200 °C and 400 °C temperatures. At 400 °C and 600 °C CoO, Cr_2O_3 phases to be found. The $CoWO_4$ and MoO_2 phases are noticed at 600 °C. In the case of coating 1 due to the presence of nickel element $NiCr_2O_4$ phase

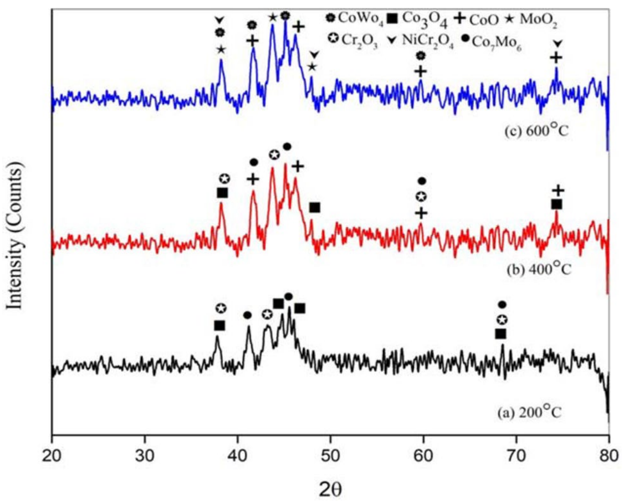

Fig. 15 XRD pattern of fused coating 1

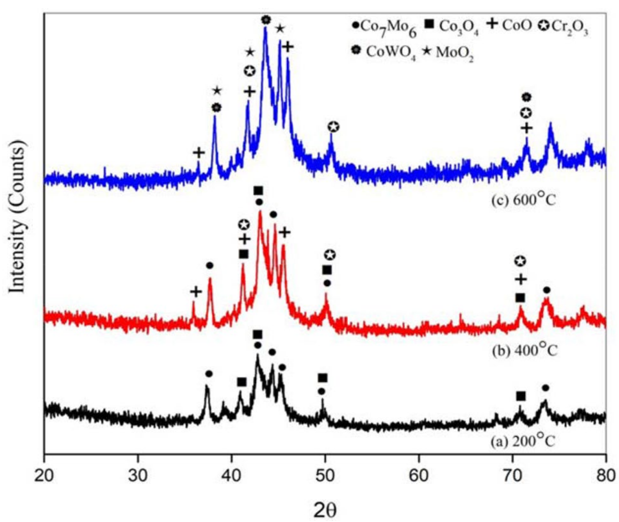

Fig. 16 XRD pattern of fused coating 2

is identified at 600 °C see in Fig. 15. The fused coating exhibits less wear rate and friction coefficient because of oxides are actively formed leads to cover the exposed coating surface from adhesive wear mechanism.

3.5.4 Microstructure Analysis of Worn Surface

3.5.4.1 Coating 1 In order to understand the wear phenomenon of coatings, worn surfaces by SEM is investigated. Figure 17a–c and d–f presents the SEM images of wear out surfaces of as-sprayed and fused coating 1 respctively. The as-sprayed worn surfaces of tested samples under 20 N normal at all test temperatures exhibits less width wear tracks associated with breaking of splats, the formation of large pits and underlying surface subjected to mild oxidation at elevated temperatures [35–37]. The presence of deep and short width wear tracks confirms transferring of alumina counterpart disc material to wear surface as shown in Fig. 17a–c. This reveals that the as-sprayed coatings with adhesive wear mechanism. The EDS results of corresponding morphologies of as-sprayed coating 1 (Fig. 17a–c) indicates the presence of oxide and alumina content and its percentage is significantly increasing as a rise in test load and temperatures. These results depend on the increase in wear rate and higher friction, other researchers have also reported the similar mechanism of higher the surface roughness and lower microhardness results in a higher material loss [38, 39].

The fused coating 1 exhibit typical worn morphologies shown in Fig. 17d–f. There is no indication of the uneven surface on worn images which is less rough and promotes to smoother sliding action under 20 N normal load. The homogeneous structure of fused coating 1 leads to protection of coatings surfaces and these surfaces are subjected to the severe oxidational phenomenon [40, 41]. The higher microhardness of fused coating 1 undergone fatigue spalling effect on all wear test samples. The percentage of alumina is little less compared to as-sprayed coating 1 and an increase in oxide content with an increase in test temperatures as noticed from EDS results of respective fused coating 1 in Fig. 17d–f. The formation of tribo oxide films on fused coating 1 surfaces eliminates the adhesive wear mechanism and improves its wear and frictional resistance [11, 22, 23].

3.5.4.2 Coating 2 Figure 18a–c shows the typical morphologies of wear tracks under 20 N normal load produced on as-sprayed coating 2. The wear scratches formed on worn surface are deeper and shorter in width results in detachment of splats occurred at all test temperatures. The wear surface has scratches caused by exfoliated carbide particles, and the wear mechanism is adhesive wear. As test temperature increases to 400 °C and 600 °C as-sprayed coating 2 experienced oxidation and breaking of oxide layers due to adhesive wear turned into material loss under 20 N normal load. EDS report confirmed the oxide elements which are developed during elevated temperature test. The oxygen content in the dark region is in the range of 15.0 to 27 wt%, because high frequency friction will significantly increase the surface temperature, and an oxide friction layer will be formed on the surface of the coating. Therefore, the oxidative wear in dry friction and wear conditions is the main wear mechanism of the coating.

Figure 18d–f presents worn micrographs of fused coating 2 under 20 N normal load. The tracks of wear are slight bigger and narrow no traces of delamination on worn surfaces. As fused coating 2 exhibits homogeneous structure which results in smooth sliding against to disc. The darker regions on fused coating 2 subjected to severe oxidation

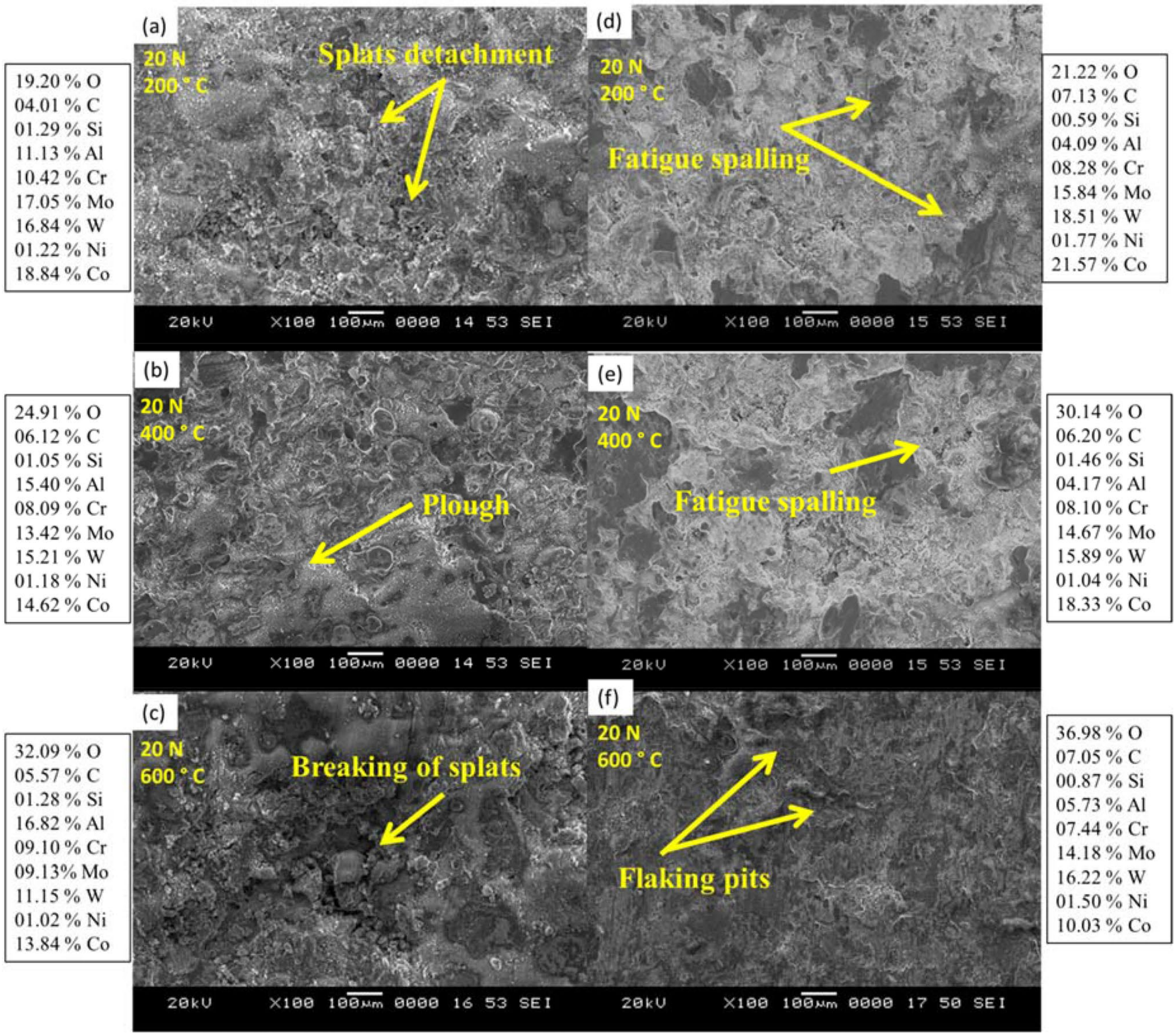

Fig. 17 SEM images of the damaged surfaces of the coating 1, **a**–**c** as-sprayed, **d**–**f** fused

at 400 °C and 600 °C tribo oxides are produced results in shielding of underlying surface [40, 41]. Fused coating 2 experienced fatigue spalling of wear mechanism in which no sign of detaching and tearing of layers [26, 42–45]. EDS analysis on the surface of a worn fused coating 2 presented in Fig. 18d–f.

The estimated wear rate coefficients K in mm^3/N-m of both tested coating 1 and 2 are represented in Fig. 19. The Archard model based equation is used on constant sliding speed with varying load and test temperatures [44]. The equation is written as $W/LC = k$, where W = wear in mm^3, L = sliding length in m, C = normal load in N. The assessed K value of CoMoCrSi/WC-CrC-Ni before and after post treated composite coatings are 4×10^{-6} mm^3/N-m and 1×10^{-6} mm^3/N-m respectively. The K value of CoMoCrSi/WC-12Co before and after post treated coatings composite coatings are 3×10^{-6} mm^3/N-m and 8×10^{-6} mm^3/N-m respectively. The CoMoCrSi/WC-12Co post treated composite coating revealed better wear resistance comparing with other coatings.

4 Conclusion

The use of milled CoMoCrSi powder provides intermetallic laves phases in the coatings which are hard in nature provides better wear resistance. Flame sprayed coatings exhibits lamellar (heterogeneous) structure with presence of unmelted/partial melted particles. Homogeneous structure with lower surface roughness is achieved in coatings due

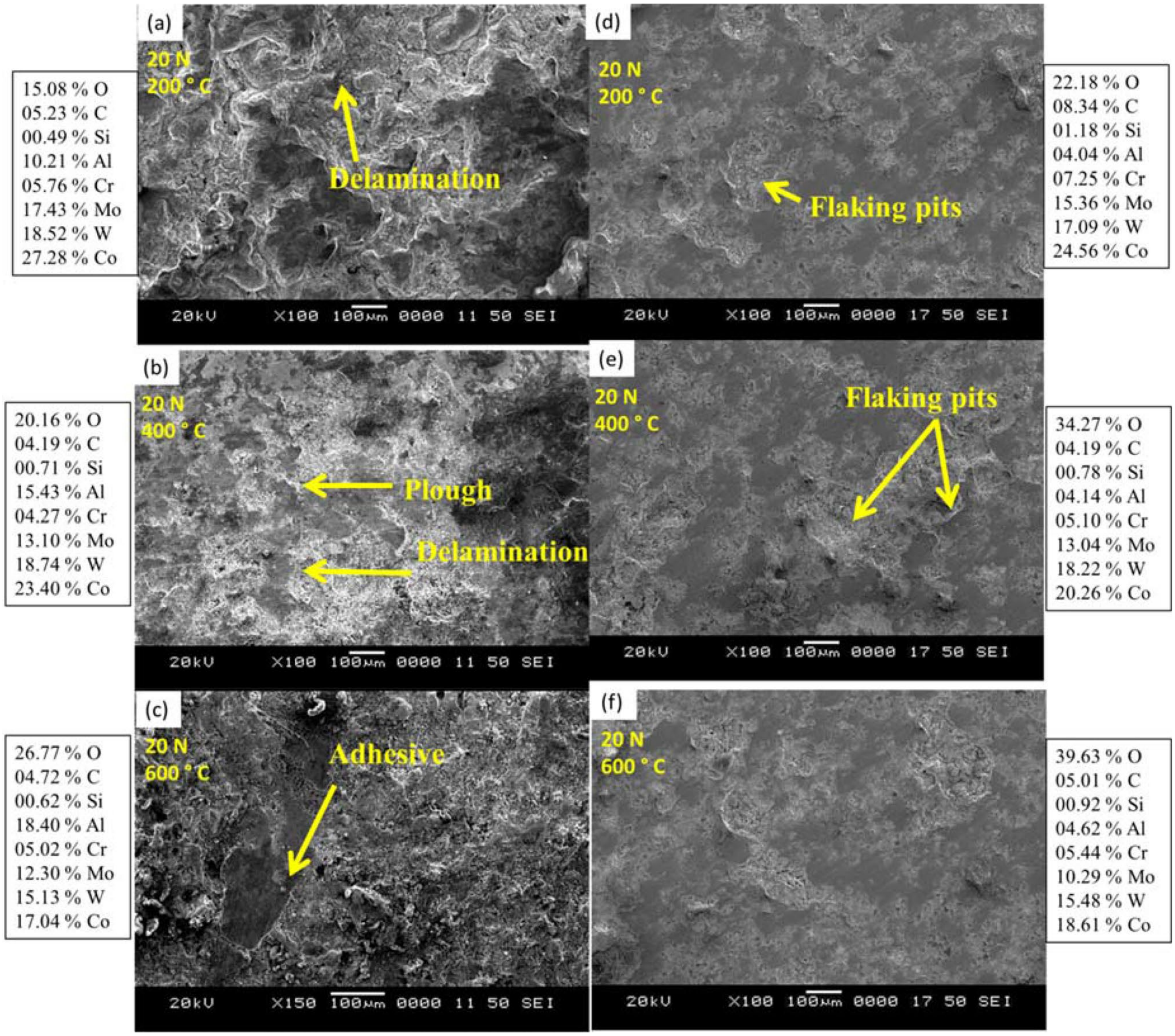

Fig. 18 SEM images of the damaged surfaces of the coating 2, **a**–**c** as-sprayed **d**–**f** fused

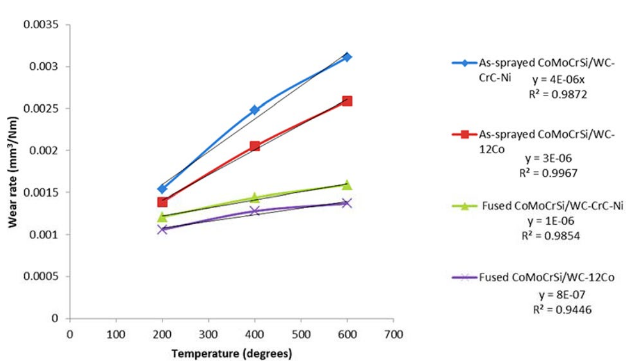

Fig. 19 Wear rate coefficient (K) of the coating 1 and coating 2

to post-heat treatment through microwave hybrid heating. The fused coating retains the similar phases as observed at as-sprayed and two new phases TiC and TiO_2 have been identified by a diffusion process. The new phases such as Co_6W_6C, Co_3W_9C, Co_3W_3C Co_3C and SiC significantly strengthen the coating hardness, high-temperature wear resistance properties. Post treatment of as-sprayed coatings by microwave energy results in the inter-diffusion of coating substrate elements and also enhanced microhardness due to metallurgical bonding.

The both post treated coating 1 and 2 exhibits lower volume loss and wear rate at 10 N and 20 N normal loads compared to both as-sprayed coatings as well as the substrate.

Co_3O_4, MoO_2, CoO, $NiCr_2O_4$, $CoWO_4$, and Cr_2O_3 oxide phases are formed. These oxide phases acts as protective shield for underlying surface during sliding action at elevated temperatures. Both post treated coating 1 and 2 revealed less wear scars results in fatigue spalling wear mechanism.

Acknowledgements The authors are thankful to Aum Techno Spray Bangalore, Karnataka, India for giving access to utilize Flame spray coating facility. No funds or grants received for this work from any sectors.

References

1. Schneider A, Gumenyuk A, Lammers M, Malletschek A, Rethmeier M (2014) Laser beam welding of thick titanium sheets in the field of marine technology. Phys Proc 56:582–590
2. Gorynin IV (1999) Titanium alloys for marine application. Mater Sci Eng A 263(2):112–116
3. Pukasiewicz AGM, de Boer HE, Sucharski GB, Vaz RF, Procopiak LAJ (2017) The influence of HVOF spraying parameters on the microstructure, residual stress and cavitation resistance of FeMnCrSi coatings. Surf Coat Technol 327:158–166
4. Miller PD, Holladay JW (1958) Friction and wear properties of titanium. Wear 2(2):133–140
5. Bemporad E, Sebastiani M, Casadei F, Carassiti F (2007) Modelling, production, and characterization of duplex coatings (HVOF and PVD) on Ti–6Al–4V substrate for specific mechanical applications. Surf Coat Technol 201:7652–7662
6. Murugan K, Ragupathy A, Balasubramanian V, Sridhar K (2014) Optimizing HVOF spray process parameters to attain minimum porosity and maximum hardness in WC–10Co–4Cr coatings. Surf Coat Technol 247:90–102
7. Lin CM, Yen SH, Su CY (2016) Measurement and optimization of atmospheric plasma sprayed CoMoCrSi coatings parameters on Ti-6Al-4V substrates affecting microstructural and properties using hybrid abductor induction mechanism. Measurement 94:157–167
8. Durga Prasad C, Joladarashi S, Ramesh MR, Sarkar A (2018) High temperature gradient cobalt based clad developed using microwave hybrid heating. Am Inst Phys Publ 1943:020111. https://doi.org/10.1063/1.5029687
9. Bergant Z, Trdan U, Grum J (2014) Effect of high-temperature furnace treatment on the microstructure and corrosion behavior of NiCrBSi flame-sprayed coatings. Corros Sci 88:372–386
10. Davies JR (2004) Handbook of thermal spray technology. ASM International, Materials Park, OH
11. Durga Prasad C, Joladarashi S, Ramesh MR, Srinath MS, Channabasappa BH (2019) Effect of microwave heating on microstructure and elevated temperature adhesive wear behavior of HVOF deposited CoMoCrSi-Cr_3C_2 composite coating. Surf Coat Technol 374:291–304
12. Kim HJ, Hwang SY, Lee CH, Juvanon P (2003) Assessment of wear performance of flame sprayed and fused Ni-based coatings. Surf Coat Technol 172(2–3):262–269
13. Cano C, Osendi MI, Belmonte M, Miranzo P (2006) Effect of the type of flame on the microstructure of $CaZrO_3$ combustion flame sprayed coatings. Surf Coat Technol 201(6):3307–3313
14. Sharma S (2014) Parametric study of abrasive wear of Co–CrC based flame sprayed coatings by response surface methodology. Tribol Int 75:39–50
15. Li J, Liao H, Coddet C (2002) Friction and wear behavior of flame-sprayed PEEK coatings. Wear 252:824–831
16. Gonzalez R, Cadenas M, Fernandez R, Cortizo JL, Rodrıguez E (2007) Wear behaviour of flame sprayed NiCrBSi coating remelted by flame or by laser. Wear 262:301–307
17. Navas C, Colaco R, de Damborenea J, Vilar R (2006) Abrasive wear behaviour of laser clad and flame sprayed-melted NiCrBSi coatings. Surf Coat Technol 200:6854–6862
18. Durga Prasad C, Joladarashi S, Ramesh MR, Srinath MS, Channabasappa BH (2019) Development and sliding wear behavior of Co-Mo-Cr-Si cladding through microwave heating. Silicon. https://doi.org/10.1007/s12633-019-0084-5
19. Zafar S, Sharma AK (2017) Microstructure and mechanical properties of microwave post-processed Ni coating. J Mater Eng Perform 26(3):382–1390
20. Bolelli G, Berger LM, Bonetti M, Lusvarghi L (2014) Comparative study of the dry sliding wear behavior of HVOF-sprayed WC–(W, Cr) 2C–Ni and WC–CoCr hard metal coatings. Wear 309:96–111
21. Harsha S, Dwivedi DK, Agrawal A (2007) Influence of WC addition in Co–Cr–W–Ni–C flame sprayed coatings on microstructure, microhardness and wear behavior. Surf Coat Technol 201:5766–5775
22. Durga Prasad C, Joladarashi S, Ramesh MR, Srinath MS, Channabasappa BH (2018) Influence of microwave hybrid heating on the sliding wear behaviour of HVOF sprayed CoMoCrSi coating. Mater Res Express 5:086519
23. Durga Prasad C, Joladarashi S, Ramesh MR, Srinath MS, Channabasappa BH (2019) Microstructure and tribological behavior of flame sprayed and microwave fused CoMoCrSi/CoMoCrSi-Cr_3C_2 coatings. Mater Res Express 6:026512
24. Bolelli G, Lusvarghi L (2006) Tribological properties of HVOF as-sprayed and heat treated Co–Mo–Cr–Si coatings. Tribol Lett 25:43–54
25. Honga S, Wu Y, Wang B, Zhang J, Zheng Y, Qiao L (2017) The effect of temperature on the dry sliding wear behavior of HVOF sprayed nanostructured WC-CoCr coatings. Ceram Int 43:458–462
26. Torres B, Campo M, Lieblich M, Rams J (2013) Oxy-acetylene flame thermal sprayed coatings of aluminium matrix composites reinforced with $MoSi_2$ intermetallic particles. Surf Coat Technol 236:274–283
27. Houdkova S, Smazalova E, Vostrak M, Schubert J (2014) Properties of NiCrBSi coating, as sprayed and remelted by different technologies. Surf Coat Technol 253:14–26
28. Kahraman N, Gulenc B (2002) Abrasive wear behaviour of powder flame sprayed coatings on steel substrates. Mater Des 23:721–725
29. Uyulgan B, Dokumaci E, Celik E, Kayatekin I, AkAzem NF, Ozdemir I, Toparli M (2007) Wear behaviour of thermal flame sprayed FeCr coatings on plain carbon steel substrate. J Mater Process Technol 190:204–210
30. Soveja A, Sallamand P, Liao H, Costil S (2011) Improvement of flame spraying PEEK coating characteristics using lasers. J Mater Process Technol 211:12–23
31. Dejuna K, Tianyuan S (2017) Wear behaviors of HVOF sprayed WC-12Co coatings by laser remelting under the lubricated condition. Opt Laser Technol 89:86–91
32. Redjdal O, Zaid B, Tabti MS, Henda K, Lacaze PC (2013) Characterization of thermal flame sprayed coatings prepared from FeCr mechanically milled powder. J Mater Process Technol 213:779–790
33. Yu HL, Zhang W, Wang HM, Yin YL, Ji XC, Zhou KB (2016) Comparison of surface and cross-sectional micro-nano mechanical properties of flame sprayed NiCrBSi coating. J Alloy Compd 672:137–146
34. Khameneh Asl Sh, Heydarzadeh Sohi M, Hokamoto K, Uemura M (2006) Effect of heat treatment on wear behavior of HVOF thermally sprayed WC-Co coatings. Wear 260:1203–1208

35. Wood PD, Evans HE, Ponton CB (2010) Investigation into the wear behavior of Tribaloy 400C during rotation as an unlubricated bearing at 600 °C. Wear 269:763–769
36. Durga Prasad C, Joladarashi S, Ramesh MR, Srinath MS, Channabasappa BH (2020) Comparison of Microstructural and Sliding Wear Resistance of HVOF Coated and Microwave Treated CoMoCrSi-WC + CrC + Ni and CoMoCrSi-WC + 12Co Composite Coatings Deposited on Titanium Substrate. Silicon. https://doi.org/10.1007/s12633-020-00398-1
37. Karaoglanli AC, Oge M, Doleker KM, Hotamis M (2017) Comparison of tribological properties of HVOF sprayed coatings with different composition. Surf Coat Technol 318:299–308
38. Gisario M, Puopolo S, Venettacci F (2015) Veniali, Improvement of thermally sprayed WC–Co/NiCr coatings by surface laser processing. Int J Refract Met Hard Mater 52:123–130
39. Asgari H, Saha G, Mohammadi M (2017) Tribological behavior of nanostructured high velocity oxy-fuel (HVOF) thermal sprayed WC-17NiCr coatings. Ceram Int 43:2123–2135
40. Xu W, Liu R, Patnaik PC, Yao MX, Wu XJ (2007) Mechanical and tribological properties of newly developed tribaloy alloys. Mater Sci Eng A 452–453:427–436
41. Zhang SH, Cho TY, Yoon JH, Li MX, Shum PW, Kwon SC (2009) Investigation on microstructure, surface properties and anti-wear performance of HVOF sprayed WC–CrC–Ni coatings modified by laser heat treatment. Mater Sci Eng B 162:127–134
42. Fang W, Cho TY, Yoon JH, Song KO, Hur SK, Youn SJ, Chun HG (2009) Processing optimization, surface properties and wear behavior of HVOF spraying WC–CrC–Ni coating. J Mater Process Technol 209:3561–3567
43. Kong D, Zhao B (2017) Effects of loads on friction wear properties of HVOF sprayed NiCrBSi alloy coatings by laser remelting. J Alloy Compd 705:700–707
44. Fernandez E, Cadenas M, Gonzalez R, Navas C, Fernandez R, de Damborenea J (2005) Wear behaviour of laser clad NiCrBSi coating. Wear 259:870–875
45. DurgaPrasad C, Jerri A, Ramesh MR (2020) Characterization and sliding wear behavior of iron based metallic coating deposited by HVOF process on low carbon steel substrate. J Bio Tribo-Corros 6:69